Koftis, Theoharris; Prinos, Panayotis; Papakyritsis, Christos

Reynolds Stress Modeling of Flow in Compound Channels with Vegetated Floodplains

ICHE 2014, Hamburg - Lehfeldt & Kopmann (eds) - © 2014 Bundesanstalt für Wasserbau ISBN 978-3-939230-32-8

Reynolds Stress Modeling of Flow in Compound Channels with Vegetated Floodplains

T. Koftis, P. Prinos & C. Papakyritsis
Hydraulics Laboratory, Department of Civil Engineering, Aristotle University of Thessaloniki, Thessaloniki, Greece

ABSTRACT: Flow in compound channel with vegetated floodplain is complex and efficient modeling of such flow should include the effects of vegetation on velocity, secondary flow and bed shear stress. In the present study, computations of the Volume-Averaged Reynolds-Averaged Navier-Stokes equations, in conjunction with a Reynolds Stress turbulence model based on a vegetation dynamics approach, are performed for a non-symmetrical compound channel of a trapezoidal main channel and a vegetated floodplain. The numerical results agree well with the available experimental data, while the model is capable to reproduce the evolution of vortices with the stronger one found in the interface region between the main channel and the vegetated floodplain. The cross-sectional flow characteristics reveal the momentum exchange mechanism between main channel and floodplain due to increased shear stresses and turbulence anisotropy near the vegetation interface. Also, the analytical SKM method of Shiono and Knight (1991) is applied for the depth-averaged velocity, together with simple Manning calculations.

Keywords: Vegetation, Compound channel, Secondary flow, Shear stress, Turbulence models

1 INTRODUCTION

In natural rivers, vegetation grows on floodplains, generating complex velocity field within the compound channel. Due to the velocity difference and the momentum exchange between the vegetated and non-vegetated area, strong shear layer and vortices occur (Liu et al. 2013). Therefore, knowledge of the mechanism of momentum exchange between the main channel and the vegetated floodplain is significant due to the effect on the discharge capacity of the channel, on erosion processes and on biological and issues.

In the present study three dimensional computations of the VARANS (Volume-Averaged Reynolds-Averaged Navier-Stokes) equations, in conjunction with a Reynolds Stress (RS) model, are performed for a non-symmetrical compound channel of a trapezoidal main channel and a vegetated floodplain, corresponding to the experimental setup of Yang et al. (2007). The drag effect of the vegetation on the current is taken into account through additional terms in both the momentum and the RSM equations based on a vegetation dynamics approach. The additional terms are related to the drag coefficient C_d and the plant density α, defined as the frontal area per unit volume (m^{-1}). The results are compared against the experiments of Yang et al. (2007). Moreover, the analytical method of Shiono and Knight (1991) is applied for the depth-averaged velocity, together with simple Manning calculations. The cross-sectional flow field is presented regarding the streamwise velocity, the shear stresses, the turbulent anisotropy and the secondary currents, revealing the momentum exchange mechanism at the interface region, between main channel and floodplain.

2 GOVERNING EQUATIONS

2.1 *Reynolds Stress Turbulent Model*

In this section the macroscopic VARANS equations are presented briefly and emphasis is given to the additional terms, due to vegetation, used in both VARANS and the Reynolds Stress (RS) turbulence model. The volume averaged continuity and momentum, equations, for fully-developed open-channel flow are written respectively as follows (Finnigan 2000, Souliotis and Prinos 2010):

$$\frac{\partial \langle U_i \rangle}{\partial x_i} = 0 \tag{1}$$

$$\langle U_j \rangle \frac{\partial \langle U_i \rangle}{\partial x_j} = -\frac{1}{\rho}\frac{\partial \langle P \rangle}{\partial x_j} + \frac{\partial}{\partial x_j}\langle -\overline{u_i u_j} \rangle - \frac{\partial}{\partial x_j}\langle \widetilde{U_i}\widetilde{U_j} \rangle + S_{mi} \tag{2}$$

where U_i = fluid velocity in the x_i direction (U, V, W in the direction x, y and z respectively), ρ = fluid density, P = effective pressure, $\langle -\overline{u_i u_j} \rangle$= Reynolds stresses and S_{mi}= extra drag term due to the presence of vegetation. The symbol $\langle \quad \rangle$ indicates averaged values over a fluid volume. The third term of the right hand side is an "additional dispersive" term, due to correlation of spatial deviations of the mean velocity components, which can be assumed negligible in flows with high vegetation density. The pressure term in Eq. (2), for the streamwise velocity U, in a channel with slope S_0 is calculated as:

$$\frac{1}{\rho}\frac{\partial \langle P \rangle}{\partial x_j} = -gS_0 \tag{3}$$

The extra drag term in Eq. (2) , is modelled according to Ayotte et al. (1999), as:

$$S_{mi} = \frac{1}{2\varphi} C_d \alpha |U| \langle U_i \rangle \tag{4}$$

where C_d= drag coefficient, α = plant density, defined as the frontal area per unit volume (m^{-1}) and φ = vegetation porosity. Similar terms, accounting for vegetation effects, are included in the transport equations of the modified Reynolds stress turbulence model, based on the Ayotte et al. (1999) model (not presented here for the sake of brevity). The extra term, used in the transport equations for the normal stresses, $S_{str.}$ is written as:

$$S_{str.} = \frac{1}{3\varphi} 0.5 C_d \alpha |\langle U \rangle|^3 \tag{5}$$

The additional dissipation term S_ε in the ε equation (ε = dissipation rate of turbulence kinetic energy), accounting for vegetation effects, is calculated as:

$$S_\varepsilon = \frac{1}{2\varphi} t_{eff}^{-1} d_{ii} \tag{6}$$

where d_{ii}= the foliage contribution associated with work against pressure and viscous drag on the vegetation (Ayotte et al. 1999) and t_{eff}= time scale variable, based on geometrical and turbulence characteristics (Uittenbogaard 2003). A more detailed analysis of the modified approach of the RSM Ayotte et al. (1999) model can be found in Souliotis and Prinos (2010).

2.2 *Analytical SKM Method*

In this section the analytical SKM is presented. Based on the momentum Eq. (2) for the streamwise velocity U, the equation for the depth-averaged velocity U_d is derived as follows:

$$\rho\left(\frac{\partial H(UW)_d}{\partial z}\right) = \rho g H S_0 + \frac{\partial H \widetilde{\tau_{xz}}}{\partial z} - \tau_b - \frac{1}{2\varphi}\rho C_d \alpha H U_d^2 \tag{7}$$

where the index d refers to depth averaged quantity, H=water depth, $\tilde{\tau}_{xz}$= turbulent shear stress, τ_b= bed shear stress. The stresses $\tilde{\tau}_{xz}$ and τ_b are calculated as $\tilde{\tau}_{xz} = \rho\tilde{\varepsilon}_{xz}\partial U_d/\partial z$, $\tau_b = (f/8)\rho U_d^2$ where $\tilde{\varepsilon}_{xz}$ is the turbulent viscosity ($\tilde{\varepsilon}_{xz} = \lambda U_* H$, λ=0.07 is turbulence constant and U_*= shear velocity) and f is the Darcy – Weisbach friction coefficient.

The left hand side of Eq. (7) denotes the secondary flow. The first term of the right hand side is the gravity term, the second term is the turbulent shear stresses, the third term is the bed shear stress and the last one is the extra drag term due to vegetation. The analytical solution to Eq. (7) is given as $U_d = (A_1 e^{\gamma z} + A_2 e^{-\gamma z} + k)^{1/2}$ where A_1 and A_2 constants (different for the vegetated and the non vegetated

region) which are determined from appropriate boundary and interfacial conditions, and γ and k are parameters, which are determined for the non-vegetated and vegetated region separately. Details of the analytical solutions can be found in Tang et al. (2011).

3 NUMERICAL IMPLEMENTATION

The dimensions of the computational domain and the hydraulic conditions used in the present study correspond to the experimental setup of Yang et al. (2007), for compound channels with emergent vegetation on the floodplain as shown in Figure 1 (left). More specifically, the flume has a bed slope S_0=1.25‰ and width B= 0.30m, while the main channel and the floodplain have width b=0.08m and 0.13m respectively. The main channel has a side slope, s_{mc}=1.5 and the bankfull height is h=0.06 m. The vegetation is represented in the experiments by plastic circular straws with diameter of d=0.004m and row spacing 0.03m and the plant spacing 0.02m, resulting in plant density α=6.67 m^{-1} and porosity φ=0.979.

The effect of the relative depth Dr, defined as $Dr=(H-h)/H$, with H=total depth flow, is investigated together with the effect of floodplain vegetation on the mean velocity and turbulent characteristics of the flow. Therefore, three different runs are performed for Dr=0.15, 0.30 and 0.56, for vegetated floodplain and for free floodplain. It is well known that momentum exchange and the interaction mechanism between main channel and floodplain flows are increased with decreasing relative depth. It should be mentioned that for the deep flow case, Dr=0.56 computed results are compared with available experimental data of Yang et al. (2007).

The FLUENT CFD code is used for the numerical computations, while the GAMBIT mesh generator is used for the construction of the grid. FLUENT uses a finite volume technique for solving the continuity and momentum equations and the transport equations for the Reynolds Stresses and the turbulent dissipation rate, ε. The extra source terms S_{mi}, S_{str} and S_{ε}, accounting for the vegetation effects are modeled using User Defined Functions (UDF). The drag coefficient C_d used in the calculation of the above mentioned terms, a function of the cylinder Reynolds number ($Re=Ud/v$, U=streamwise velocity, d = cylinder diameter, v=fluid viscosity) and the dimensionless array density, ad. For ad<0.03 as in the present study (ad=0.0267) the relationship $C_d = 1 + 10.0Re^{-2/3}$, proposed by White (1991), is reasonable. Applying the above equation for the hydraulic conditions of Table 1, an average indicative value of C_d~ 1, is used in the present study.

GAMBIT is used for the construction of a three-dimensional grid with orthogonal shaped cells. In order to avoid the increased length, needed for the flow to become fully developed, periodic conditions are used in the streamwise direction. Wall boundary conditions are applied for the channel side walls and the flume bed, while the free surface is simulated as a symmetry axis (low Froude number). The grid used was non-uniform, while the dimensions of the cells varied as Δx=2mm, Δz=1.48-2.00mm and Δy=1.00-1.79mm (streamwise, lateral and vertical direction, respectively). For the highest relative depth, Dr=0.56, the grid size was 5x171x76 resulting in 64980 computational cells. For the lower relative depth runs, Dr=0.30 and Dr=0.15, 44460 cells and 18810 cells where used respectively. The numerical three-dimensional grid is depicted in Figure 1 (right).

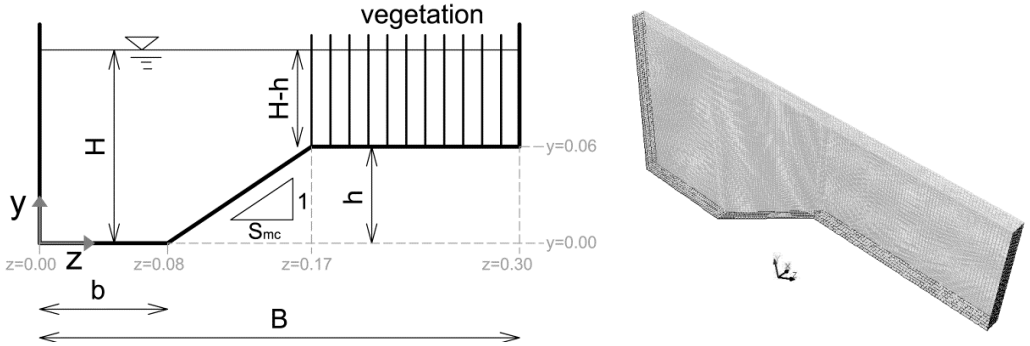

Figure 1. Cross-section of the compound channel with vegetated floodplains (left) and numerical 3D domain (right)

The results for the calculated velocities in the main channel, floodplain and the cross-section (indicator *mc*, *fl* and *mean* respectively) are shown in Table 1, together with different Manning calculations (a) Separate channels method with a vertical interface between main channel and floodplain (SeCM-VI), (b) Separate channels method with a horizontal interface (SeCM=HI) and (c) the Single channel method (SiCM).

From the results it appears that SKM predicts higher velocities than the numerical results in both the main channel and the floodplain for all cases. It is also shown that increasing relative depth, results in increasing flow velocities of the cross-section U_{mean} for the free floodplain cases and decreasing ones for the vegetated floodplain, which is in accordance with the Yang et al. (2007) experiments. Regarding the Manning calculation, the SeCM-VI seems to give better results as compared with the numerical and SKM velocities for the lower relative depths (Dr=0.15 and 0.30), while for the high relative depth (Dr=0.56) the SiCM gives the better estimation of the flow velocity.

The velocities within the vegetated floodplain are quite similar for both the numerical and SKM results and in good agreement with the simple proposed analytical solution, $U = \sqrt{2gS/C_d\alpha}$ of White and Nepf (2008), which however does not take into account the flow depth.

Table 1. Cases examined and velocities from numerical (FLUENT), analytical (SKM) and different Manning calculations

U(m/s)			FLUENT			SKM			SeCM-VI			SeCM-HI	SiCM
Case	$H(m)$	Dr	U_{mc}	U_{fl}	U_{mean}	U_{mc}	U_{fl}	U_{mean}	U_{mc}	U_{fl}	U_{mean}	U_{mean}	U_{mean}
Free1	0.071	0.15	0.415	0.141	0.379	0.493	0.169	0.450	0.387	0.166	0.358	0.322	0.318
Free2	0.086	0.30	0.466	0.287	0.427	0.535	0.261	0.474	0.437	0.275	0.401	0.389	0.382
Free3	0.136	0.56	0.601	0.571	0.590	0.621	0.406	0.551	0.560	0.466	0.530	0.582	0.525
Veg1	0.071	0.15	0.392	0.060	0.348	0.490	0.067	0.434	0.376*	0.061	0.335		
Veg2	0.086	0.30	0.369	0.074	0.304	0.521	0.076	0.423	0.411*	0.061	0.334		
Veg3	0.136	0.56	0.334	0.082	0.252	0.538	0.088	0.368	0.487*	0.061	0.348		

* The vertical interface has been taken into account for the calculation of the wetted perimeter.

4 ANALYSIS OF RESULTS

4.1 *Streamwise Velocity and Shear Stresses*

The numerical model is validated against the available experimental results of Yang et al. (2007) for the cases with Dr=0.56 (high relative depth, weak interaction mechanism) for both vegetated and free floodplains. Figure 2 shows the velocity distribution (made dimensionless with the average cross-sectional velocity U_{mean}) at different locations for Dr=0.56 and non-vegetated floodplain. The numerical results are in quite good agreement with the experimental data and for all cases they seem to follow the distribution of the law of the wall. However the numerical model overestimates the velocities below $Hr=y/H$=0.3 for almost all locations. The same comparison for the vegetated floodplain case is shown in Figure 3. The experimental velocities follow an S-shaped distribution at all locations, which is not reproduced by the numerical results. However except the location z=17cm (the vertical interface between the main channel and floodplain, the numerical results predict quite well the velocity distribution.

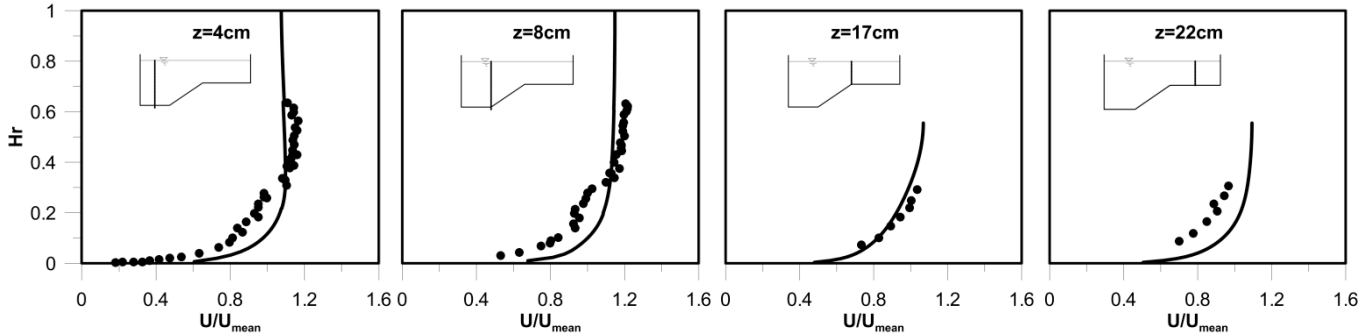

Figure 2. Vertical distribution of velocity (U/U_{mean}) at different locations for Dr=0.56 and free floodplain for numerical (solid line) and experimental data of Yang et al. 2007 (dots).

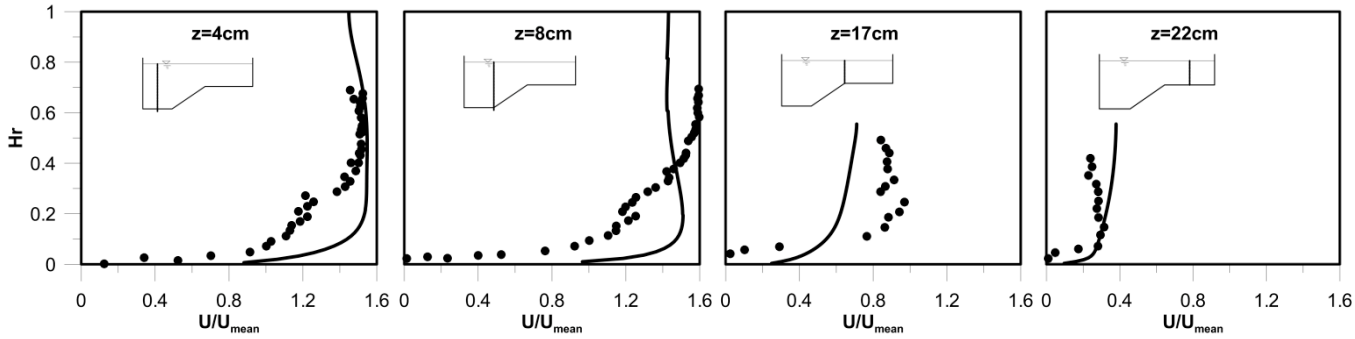

Figure 3. Same as Figure 2 for *Dr*=0.56 and vegetated floodplain.

The numerical and analytical depth-averaged velocity profiles, made dimensionless with the cross-sectional velocity U_{mean}, are shown in Figure 4 for the free and vegetated floodplain together with experimental data of Yang et al. (2007) for *Dr*=0.56 (vegetated floodplain). It appears that the SKM overestimates the velocities in the main channel for all cases, and also exhibits a sharp edge in the maximum velocity at the beginning of the side slope, which is not the case for the numerical results. For the vegetated cases the distribution of numerical velocities is in good agreement with the experimental data. The main reason for the weakness of the SKM method to efficiently describe the velocity distribution is the 3-D character of the flow since the method is usually applied for shallow flow conditions (*B/H*>10) where secondary flow is insignificant, which is not the case in the present study (*B/H*= 2.2-4.2). Also, for the vegetated cases, the deviation could be attributed to the weakness of the depth-averaged analytical model to efficiently describe the momentum exchange between the main channel and the vegetated floodplain.

Such momentum exchange for the vegetated floodplain cases is evident in Figure 5, where the distribution of the depth averaged Reynolds stresses $-\overline{uw}$ (made dimensionless with the friction velocity, as calculated by $\overline{U}_*^2 = \rho g R_h S_o$) is shown for the numerical results. Near the vertical interface (*z/B*=0.56) increased stresses are computed for the vegetated floodplain cases accounting for the momentum exchange between the vegetated and non-vegetated zone.

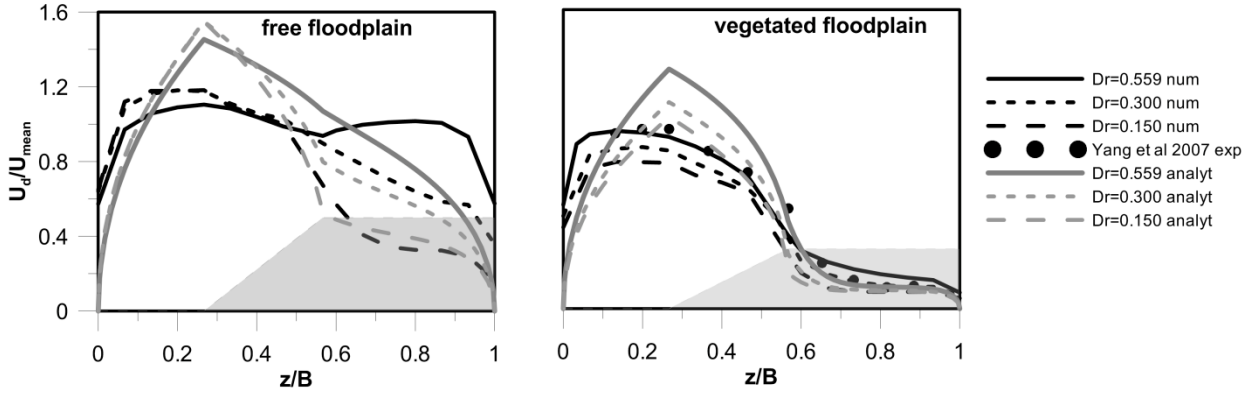

Figure 4. Distribution of depth averaged velocity (U_d/U_{mean}) for all cases with (a) free and (b) vegetated floodplain.

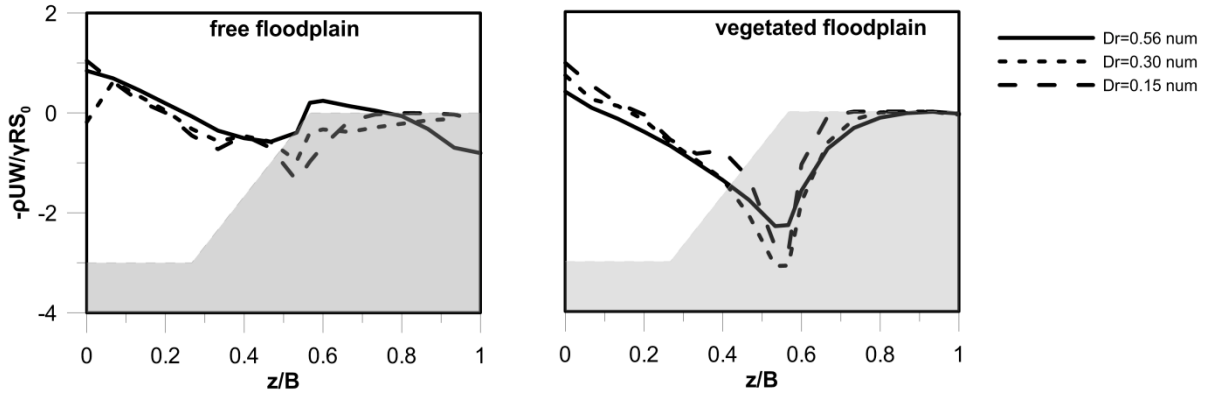

Figure 5. Distribution of depth averaged Reynolds stresses $-\overline{uw}/\overline{U}_*^2$ for all cases with (a) free and (b) vegetated floodplain.

4.2 *Cross-sectional Characteristics*

In this section the cross-sectional flow characteristics for *Dr*=0.15 and 0.30 and vegetated floodplains are presented in terms of dimensionless velocities (either the average velocity of the channel cross-section U_{mean}, or the friction velocity $\overline{U}_*$ calculated analytically as $\overline{U}_*^2 = \rho g R_h S_o$). Figure 6 shows the streamwise velocities where it is shown that the velocity contours in the main channel are similar to those of an open channel-flow with the vertical interface acting as the right channel "wall" with increased shear. The contours within the vegetated floodplain tend to be parallel to the bed and much smaller than those in the main channel. Figure 7 present the shear stresses $-\overline{uv}/\overline{U}_*^2$ due to velocity gradients in the vertical direction revealing the effect of the slide slope of the main channel in the flow field. Local maxima are shown in the corners of the side slope, while in the vegetated floodplain the stresses diminish. The shear stresses due to velocity gradients in the lateral direction $-\overline{uw}/\overline{U}_*^2$ are depicted in Figure 8. The values of $-\overline{uw}$, near the vertical interface are much higher than those of $\overline{U}_*^2$, indicating that the vertical interface exerts much higher resistance to the channel flow that that of the channel bed and the side wall. Hence, such a shear has to be estimated accurately for the correct determination of the channel velocity and the carrying capacity of such channels. It is also shown that increasing relative depth results in higher penetration of stresses within the floodplain.

For three-dimensional flows, such as in the tested cases, secondary currents are generated by the anisotropy of turbulence$\left(\overline{w^2} - \overline{v^2}\right)$, as suggested by Nezu and Nakagawa (1984), which are significant near the vertical interface as shown in Figure 9. The secondary currents are depicted in Figures 10, 11 and 12 for all the examined cases, with vectors of the normalized vertical and spanwise mean velocities, V/U_{mean} and W/U_{mean} respectively. It is shown that the magnitude of the secondary flow is considerable especially in the main channel near the vertical interface, with higher values obtained for the high relative depth (*Dr*=0.56) and for the vegetated floodplain (~8% of U_{mean}). Also a steady vortical structure is observed, which for *Dr*=0.56 is similar to the experimental one of Yang et al. (2007), with clockwise and anticlockwise vortices shown especially for the vegetated floodplain cases, with the stronger one found in the interface region.

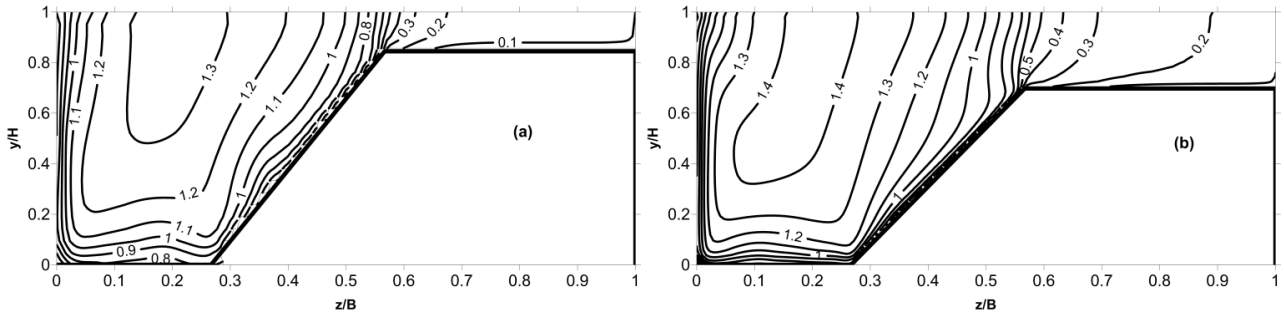

Figure 6. Contours of streamwise velocity U/U_{mean} for vegetated floodplain cases (a) *Dr*=0.15, (b) *Dr*=0.30.

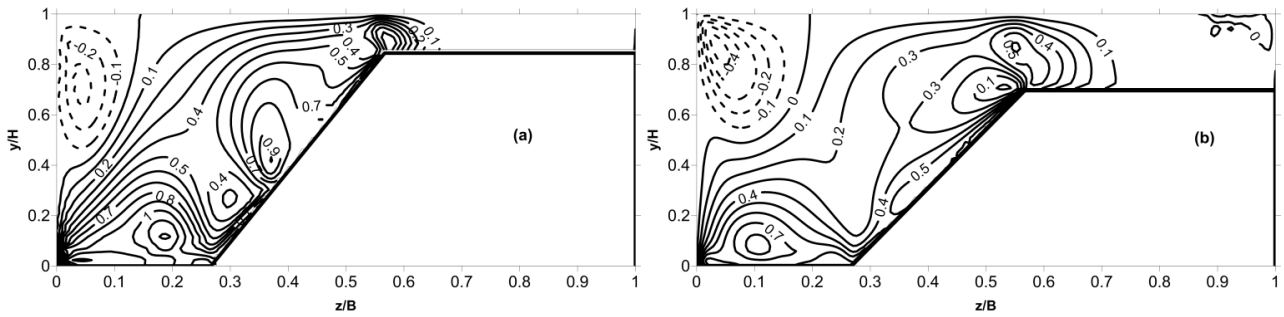

Figure 7. Contours of shear stress $-\overline{uv}/\overline{U}_*^2$ for vegetated floodplain cases (a) *Dr*=0.15, (b) *Dr*=0.30.

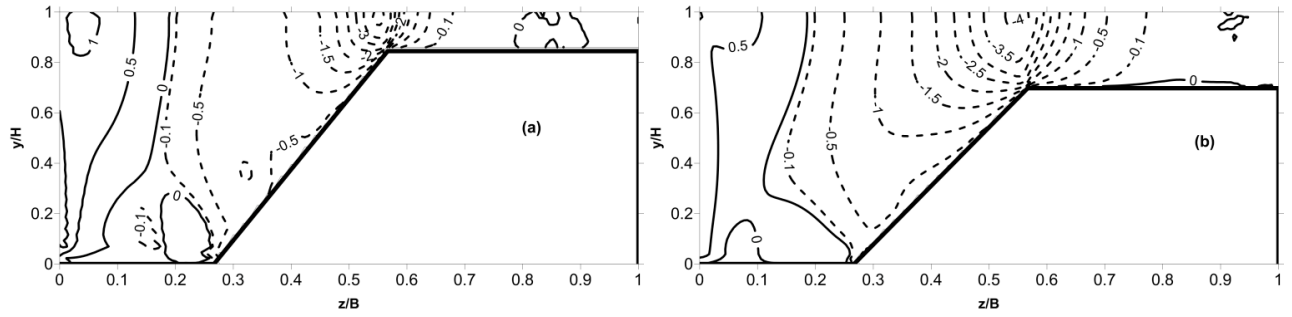

Figure 8. Contours of shear stress $-\overline{uw}/\bar{U}_*^2$ for vegetated floodplain cases (a) *Dr*=0.15, (b) *Dr*=0.30.

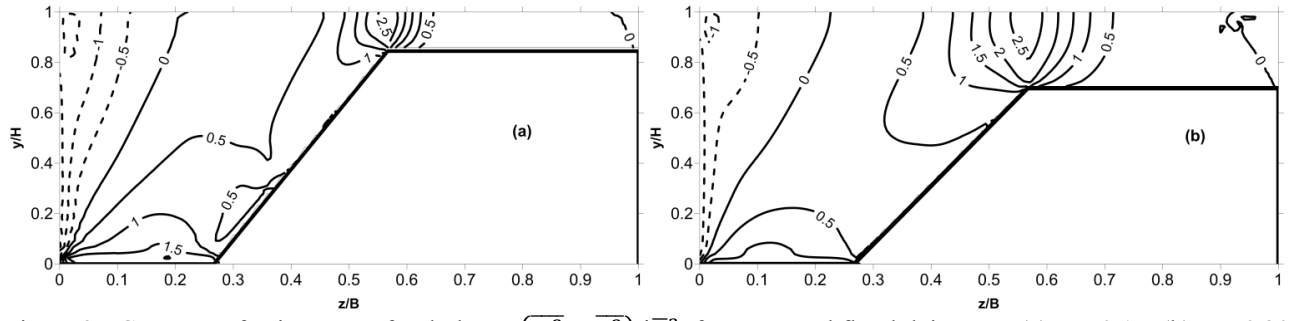

Figure 9. Contours of anisotropy of turbulence $\left(\overline{w^2}-\overline{v^2}\right)/\bar{U}_*^2$ for vegetated floodplain cases (a) *Dr*=0.15, (b) *Dr*=0.30.

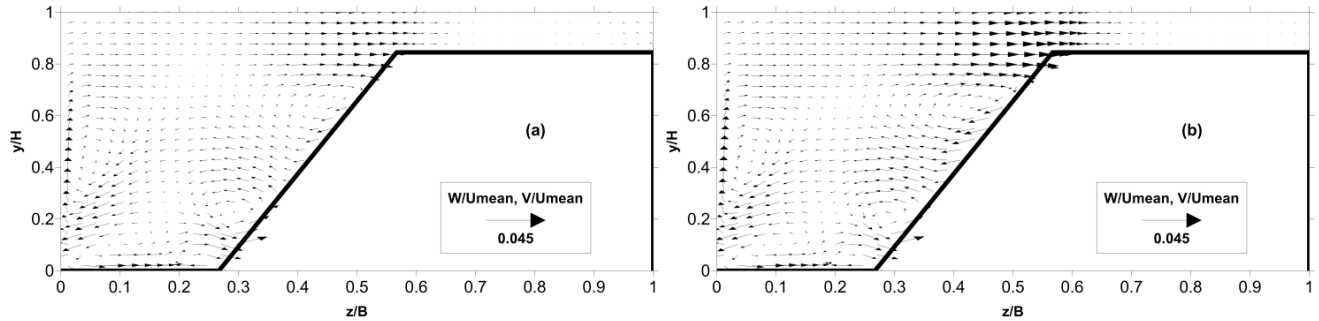

Figure 10. Vectors of secondary currents velocity V/U_{mean}, W/U_{mean} for *Dr*=0.15 with (a) free and (b) vegetated floodplain.

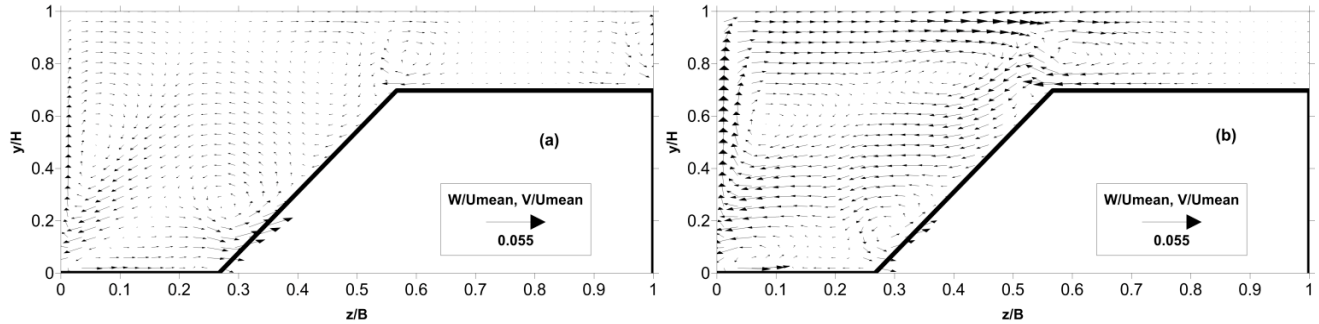

Figure 11. Vectors of secondary currents velocity V/U_{mean}, W/U_{mean} for *Dr*=0.30 with (a) free and (b) vegetated floodplain.

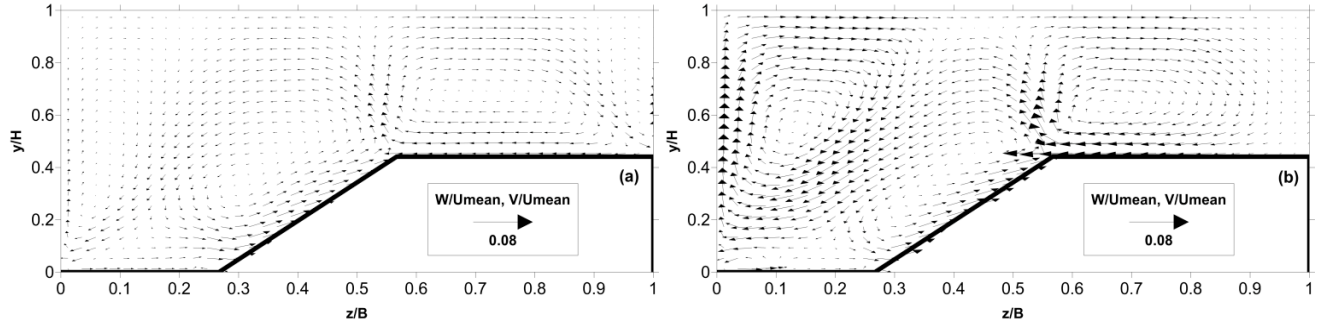

Figure 12. Vectors of secondary currents velocity V/U_{mean}, W/U_{mean} for *Dr*=0.56 with (a) free and (b) vegetated floodplain

5 CONCLUSIONS

The main conclusions from the numerical study of Reynolds stress modeling of flow in compound channels with vegetated floodplains can be summarized in the following:

- The turbulence penetration through the vegetation interface is evident with increased stresses and turbulence anisotropy near the vegetation interface, due to the momentum exchange between main channel and floodplain.
- The secondary flow is considerable especially in the main channel near the vertical interface with the vegetated floodplain (~8% of U_{mean}). The numerical model is able to reproduce the evolution of vortices with the stronger one found in the interface region. The vortical pattern is in accordance with the experimental findings of Yang et al. (2007).
- The analytical SKM method overestimates the mean velocities of such channels and the depth averaged velocity profiles is not efficiently reproduced near the vertical interface due to the weakness of the model to describe accurately the momentum exchange between the main channel and the vegetated floodplain.
- The separate channels method, based on the vertical interface, estimates better the mean velocity, in comparison with the numerical one, for the lower relative depths (Dr=0.15 and 0.30), while for the higher one (Dr=0.56) the simple channel method estimates better the mean velocity.

NOTATION

α	plant density, defined as the frontal area per unit volume (m^{-1})
γ	parameter used in the SKM method for the non vegetated region
ε	dissipation rate of turbulence kinetic energy
$\widetilde{\varepsilon_{xz}}$	turbulent viscosity
λ	turbulence constant =0.07
ν	fluid viscosity
ρ	fluid density
$\widetilde{\tau_{xz}}$	turbulent shear stress
τ_b	bed shear stress
φ	vegetation porosity
$\Delta x,\Delta y,\Delta z$	dimensions of the computational cells the direction x, y and z respectively
b	main channel width
d_{ii}	the foliage contribution associated with work against pressure and viscous drag on the vegetation
d	vegetation cylinder diameter
f	Darcy – Weisbach friction coefficient
g	gravity acceleration
h	main channel bankfull height
k	parameter used in the SKM method for the vegetated region
s_{mc}	main channel side slope
t_{eff}	time scale variable used for calculation of S_ε
$\langle-\overline{u_i u_j}\rangle$	Reynolds stresses
A	cross sectional area of flow
A_1, A_2	constants used in the SKM method for the vegetated and the non vegetated region
B	channel width
C_d	drag force coefficient
Dr	relative depth ratio (H-h/H)
H	total depth flow
P	effective pressure
P_h	wetted perimeter
R_h	hydraulic radius (A/P_h)
Re	Reynolds number
S_0	channel bed slope
S_{mi}	extra drag term in momentum equation due to the presence of vegetation
S_{str}	extra term in transport equations of the Reynolds normal stresses
S_ε	extra drag term in transport equation of dissipation rate of turbulence kinetic energy
U, V, W	fluid velocity in the direction x, y and z respectively
U_d	depth averaged streamwise velocity
U_{mean}	average velocity of the channel cross-section
U_*	friction velocity

REFERENCES

Ayotte, K.W., Finnigan, J.F., Raupach, M.R. (1999). A second-order closure for neutrally stratified vegetative canopy flow. Boundary Layer Meteorology, Vol. 90, pp. 189-216.

Finnigan, J. (2000). Turbulence in plant canopies. Annual Review of Fluid Mechanics, Vol. 32, pp. 519-571.

Liu, Ch., Luo, X., Liu, X., Yang, K. (2013). Modeling depth-averaged velocity and bed shear stress in compound channels with emergent and submerged vegetation. Advances in Water Resources, Vol. 60, pp. 148-159.

Nezu, I, Nakagawa, H. (1984). Cellular Secondary Currents in Straight Conduit. Journal of Hydraulic Engineering, Vol. 110, pp. 173–193.

Shiono, K., Knight, D. (1991). Turbulent open-channel flows with variable depth across the channel. Journal Of Fluid Mechanics, Vol. 222, pp. 617-646.

Souliotis D., Prinos P. (2010). 3-D Numerical computations of turbulence in a partially vegetated shallow channel. Riverflow 2010 - Proceedings of the International Conference on Fluvial Hydraulics, Braunschweig, Germany. Andreas Dittrich Editor, pp. 83-90

Tang, X.N., Knight D.W., Sterling M. (2011). Analytical model of streamwise velocity in vegetated channels. Proceedings of the ICE - Engineering and Computational Mechanics, Vol. 164, pp. 91 –102.

Uittenbogaard, R. (2003). Modelling turbulence in vegetated aquatic flows. In Proceedings of: Riparian Forest Vegetated Channels Workshop, Trendo, Italy.

Yang K.J., Cao S.Y., Knight D.W. (2007). Flow patterns in compound channels with vegetated floodplains. Journal of Hydraulic Engineering, Vol. 133, pp. 148–159.

White, F. M. (1991). Viscous Fluid Flow, 2nd edition, McGraw-Hill, New York, USA, 614 pages.

White, B., Nepf, H. (2008). A vortex-based model of velocity and shear stress in a partially vegetated shallow channel. Water Resources Research, 44, W01412, pp. 1-15.